Article

Cell Reports

Therapeutic Potential of Patient iPSC-Derived iMelanocytes in Autologous Transplantation

Graphical Abstract

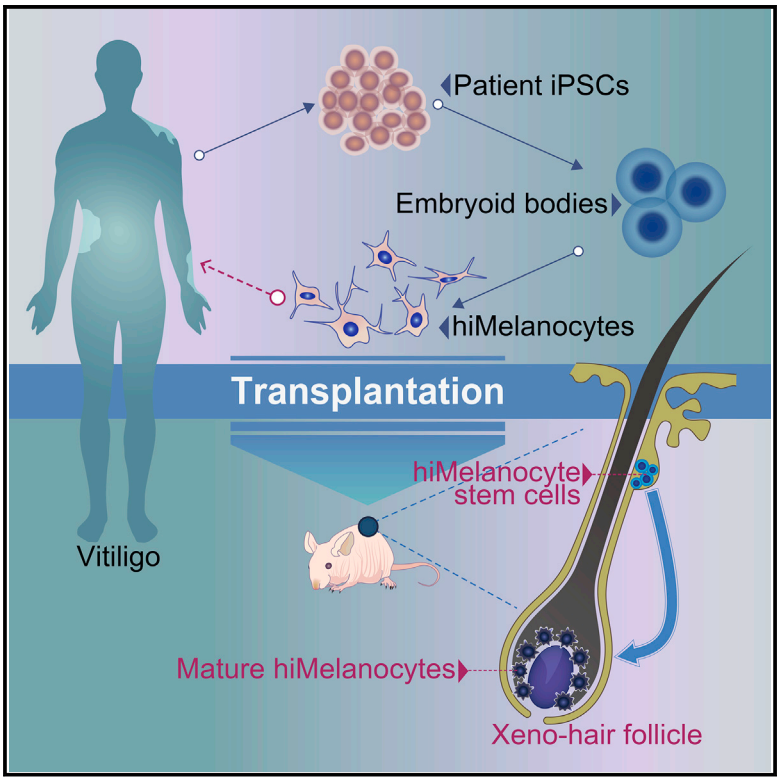

Highlights

- Suspensive system enhances efficiency of hiPSC differentiation into melanocytes
- hiMelanocyte stem cells in bulge region provide long-term function maintenance
- Mature hiMelanocytes integrate into the mouse hair bulb and produce melanin
- Patient iMelanocytes reveal multiple vitiligo-associated signaling pathways

Authors

Li-Ping Liu, Yu-Mei Li, Ning-Ning Guo, ..., Hui Xu, Lijian Hui, Yun-Wen Zheng

Correspondence

l.yumei@aliyun.com (Y.-M.L.), ljhui@sibcb.ac.cn (L.H.), ywzheng@md.tsukuba.ac.jp (Y.-W.Z.)

In Brief

Liu et al. show that patient iPSC-derived melanocytes maintain long-term functionality in mice by integrating into regions normally containing mature melanocytes and melanocyte stem cells and reconstituting pigmented hair follicles. These insights provide an alternative source for personalized cellular therapy for depigmentation.

Liu et al., 2019, Cell Reports *27*, 455–466
April 9, 2019
https://doi.org/10.1016/j.celrep.2019.03.046

CellPress

Cell Reports
Article

Therapeutic Potential of Patient iPSC-Derived iMelanocytes in Autologous Transplantation

Li-Ping Liu,[1,2,3,8] Yu-Mei Li,[1,2,8,*] Ning-Ning Guo,[1,2] Shu Li,[1,2] Xiaolong Ma,[4] Yi-Xuan Zhang,[1,2] Yimeng Gao,[4] Jian-Ling Huang,[1,2] Dong-Xu Zheng,[3] Lu-Yuan Wang,[1,2] Hui Xu,[1,2] Lijian Hui,[4,5,6,*] and Yun-Wen Zheng[1,3,7,9,*]

[1]Institute of Regenerative Medicine, Affiliated Hospital of Jiangsu University, Jiangsu University, Zhenjiang, Jiangsu 212001, China
[2]Department of Dermatology, Affiliated Hospital of Jiangsu University, Jiangsu University, Zhenjiang, Jiangsu 212001, China
[3]Faculty of Medicine, University of Tsukuba, Ibaraki 305-8575, Japan
[4]State Key Laboratory of Cell Biology, Shanghai Institute of Biochemistry and Cell Biology, Shanghai Institutes for Biological Sciences, Chinese Academy of Sciences, University of Chinese Academy of Science, Shanghai 200031, China
[5]School of Life Science and Technology, Shanghai Tech University, Shanghai 201210, China
[6]Stem Cell and Regenerative Medicine Innovation Academy, Beijing 100101, China
[7]School of Medicine, Yokohama City University, Yokohama 236-0004, Japan
[8]These authors contributed equally
[9]Lead Contact
*Correspondence: l.yumei@aliyun.com (Y.-M.L.), ljhui@sibcb.ac.cn (L.H.), ywzheng@md.tsukuba.ac.jp (Y.-W.Z.)
https://doi.org/10.1016/j.celrep.2019.03.046

SUMMARY

Induced pluripotent stem cells (iPSCs) are a promising melanocyte source as they propagate indefinitely and can be established from patients. However, the *in vivo* functions of human iPSC-derived melanocytes (hiMels) remain unknown. Here, we generated hiMels from vitiligo patients using a three-dimensional system with enhanced differentiation efficiency, which showed characteristics of human epidermal melanocytes with high sequence similarity and involved in multiple vitiligo-associated signaling pathways. A modified hair follicle reconstitution assay *in vivo* showed that MITF^{+}PAX3^{+}TYRP1^{+} hiMels were localized in the mouse hair bulb and epidermis and produced melanin up to 7 weeks after transplantation, whereas MITF^{+}PAX3^{+}TYRP1^{-} hiMelanocyte stem cells integrated into the bulge-subbulge regions. Overall, these data demonstrate the long-term functions of hiMels *in vivo* to reconstitute pigmented hair follicles and to integrate into normal regions for both mature melanocytes and melanocyte stem cells, providing an alternative source of personalized cellular therapy for depigmentation.

INTRODUCTION

Melanocytes are derived from the neural crest and are the only cell type producing melanin that protects skin cells against damage from ultraviolet radiation. Consequently, the absence of functional melanocytes leads to depigmentation disorders such as vitiligo. The estimated worldwide prevalence of vitiligo is 0.5%–1% (Ezzedine et al., 2015) and nearly 70%–80% of patients present with the condition before 30 years of age (Sehgal and Srivastava, 2007). The quality of life of patients with vitiligo is negatively affected because of the amelanotic skin (Hedayat et al., 2016; Lilly et al., 2013; Paşca et al., 2015), resulting in various psychological problems such as stress, embarrassment, anxiety, and effects of stigma. As a result, some patients with vitiligo have low self-esteem and experience social isolation (Ezzedine et al., 2015; Picardo et al., 2015).

Various types of interventions have been developed to achieve repigmentation of vitiligo, including a number of dermatosurgery techniques such as suction blister grafting, split-thickness skin grafting, punch grafting, follicular grafting, and melanocyte transplantation (Rusfianti and Wirohadidjodjo, 2006). Surgical therapies can be effective for patients with stable symptoms (Barman et al., 2004; Linthorst Homan et al., 2012; Wind et al., 2011). However, suction blister grafts and other types of tissue grafting may lead to the precipitation of new areas of vitiligo at donor sites due to the Koebner phenomenon (Whitton et al., 2015). By contrast, melanocyte transplantation is a promising therapy that is less frequently associated with adverse events and provides superior cosmetic results for patients (Mulekar and Isedeh, 2013).

Melanocytes can be isolated directly from the epidermis; however, the restricted quantity and poor proliferative capability have limited their application in cellular transplantation. Therefore, it is still a challenge to obtain large quantities of autologous melanocytes to treat patients with extensive lesions. Aside from the epidermis, there are some other potential sources for melanocytes generation, such as melanocyte stem cells and melanoblasts (Cook et al., 2005; Goldstein et al., 2015), dermal stem cells (Kumar et al., 2016b; Li et al., 2010), hair follicle stem cells (Kumar et al., 2016a), stem cells of the hair follicle outer root sheath (Schneider et al., 2014), embryonic neural crest stem cells (Shakhova and Sommer, 2015), and embryonic stem cells (ESCs) (Fang et al., 2006). Additionally, functional melanocytes can also be induced from fibroblasts and keratinocytes by direct reprogramming (Fehrenbach et al., 2016; Kazantseva et al., 2016; Yang et al., 2014). Compared with these sources, induced pluripotent stem cells (iPSCs) have significant advantages that make them ideal for generating patients' autologous melanocytes. Owing to their unlimited proliferation potential, iPSCs could provide a large quantity of melanocytes; moreover, sample collection is minimally invasive or completely noninvasive.

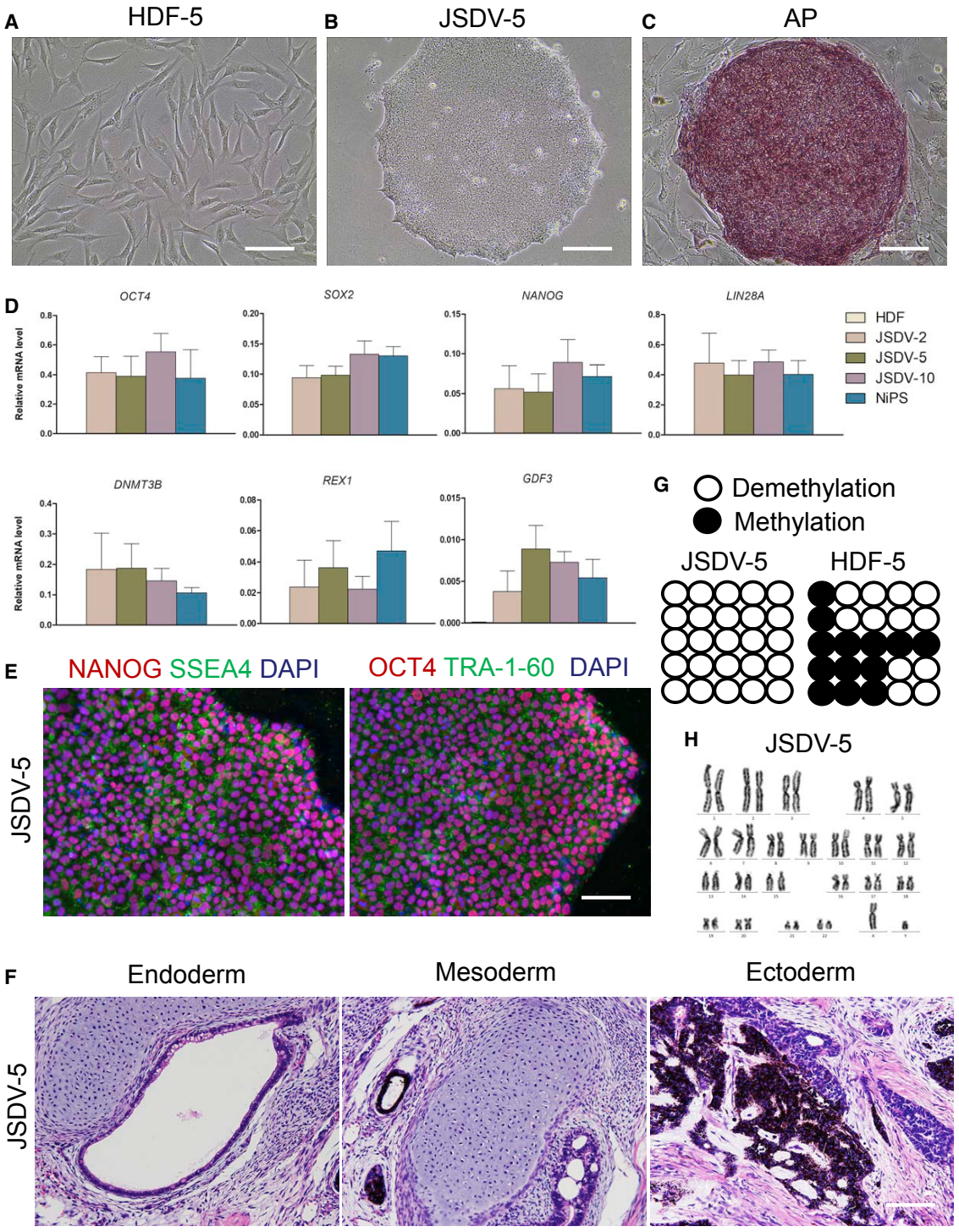

Figure 1. Establishment of iPSCs from Patient Fibroblasts

(A) Morphology of dermal fibroblasts derived from a white patch of a patient with vitiligo (N5).

(B) Morphology of induced pluripotent stem cell (iPSC) lines (JSDV-5) of patient N5.

(C) Alkaline phosphatase staining results.

(D) qPCR results showing the expression of human embryonic stem cell (hESC) marker genes in human dermal fibroblasts (HDF), Jiangsu dermal vitiligo (JSDV) cells (from patients N2, N5, and N10), and NiPSCs (iPSCs from healthy controls). Bars represent the relative quantity normalized to *GAPDH* (mean ± SD) calculated from each iPSC clone at three different passages.

(E) Immunostaining for hESC markers.

(legend continued on next page)

Another advantage of the application of iPSCs is fewer ethical concerns compared to the use of ESCs. More importantly, because genetically compatible iPSCs can be established from individual patients, drug screening could be performed within a personalized system to determine the most appropriate medical treatments for each of the affected individuals in the near future.

Previous studies indicated that iPSCs can be differentiated toward the melanocyte lineage (Jones et al., 2013; Nissan et al., 2011; Ohta et al., 2011), and these human iPSC-derived melanocytes (hiMels) could express characteristic melanocytic markers, generate melanosomes, and integrate appropriately into the reconstructed epidermis *in vitro*. However, the *in vivo* functions and the hair follicle and epidermis reconstitution capability of hiMels have not been confirmed.

Accordingly, in this study we established iPSC lines from patients with vitiligo and generated hiMels using a three-dimensional (3D) differentiation system. Moreover, to explore the potential pathogenesis of vitiligo we performed RNA sequencing and a bioinformatics assay to identify the significant pathways enriched in patient iMels. Finally, to confirm the *in vivo* functions of hiMels, we modified the conventional hair follicle reconstitution assay and transplanted the cells into immunodeficient mice.

RESULTS

Establishment of Patient-Specific iPSCs

Skin biopsies were performed in patients with vitiligo (Figure S1A). Histological examinations, including hematoxylin and eosin, 3,4-L-dihydroxyphenylalanine (L-DOPA), and Masson-Fontana staining, showed that melanocytes were absent in depigmented regions but were still present in the adjacent normal skin (Figures S1B–S1D). The expression levels of genes typical for mature melanocytes, such as *TYR*, *TYRP1*, and *DCT*, were significantly lower in the white lesion area compared with those in healthy skin (Figure S1E).

Patient iPSC lines (Jiangsu dermal vitiligo; JSDV) were established from dermal fibroblasts (Figure 1A) isolated from depigmented regions using Yamanaka factors (*OCT3/4*, *SOX2*, *KLF4*, and *c-MYC*). Non-integrating reprogramming was also conducted using RNA-based protocols (Figure S1K). These patients' clones presented morphological characteristics that were largely similar to those of human ESCs (Figures 1B, S1F, and S1L) and showed high levels of alkaline phosphatase (AP; Figures 1C and S1G). The expression levels of ESC-specific marker genes such as *OCT4*, *SOX2*, *NANOG*, *LIN28A*, *DNMT3B*, *REX1*, and *GDF3* were also comparable to those of iPSCs established from healthy individuals (Figure 1D). Specific multipotential markers, including NANOG, SSEA4, OCT4, and TRA-1-60, were also detectable by immunofluorescence staining (Figures 1E and S1M). When transplanted to mice with severe combined immunodeficiency, JSDV cells showed multipotential to form teratomas that comprised tissues of three germ layers, including the gut epithelium, muscle, cartilage tissue, neural tissue, and pigment cells (Figures 1F, S1H, S1N, and S1O). Bisulfite genomic sequencing analysis showed that the *OCT4* promoter was highly demethylated in JSDV cells whereas it was hypermethylated in parental dermal fibroblasts, further verifying the reprogramming of fibroblasts (Figures 1G and S1I). Additionally, these cell lines had a normal karyotype after dozens of passages (Figures 1H and S1J). Overall, these data confirmed the successful establishment of iPSC lines from vitiligo patients with the expected characteristics of ESCs.

Suspensive System for Melanocyte Differentiation

An embryoid body (EB)-based protocol was used to generate patient iMels; however, the differentiation efficiency of the conventional method (Ohta et al., 2011) was not satisfactory. In the conventional two-dimensional (2D) culture system, the majority of cells maintained an epithelial shape and were not differentiated into melanocytes (Figures S2A–S2C). To reduce the ratio of epithelium-like cells and improve the differentiation efficiency, we optimized the conventional method and established a suspensive system (Figure 2A). First, single-cell suspensions (Figure 2B) were prepared to generate uniform EBs (Figure 2C) using a 3D micro-culture pattern. After 5–10 days of culture, enlarged EBs (Figure 2D) were transferred into melanocyte differentiation medium on ultra-low attachment plates and suspensive induction was initiated. Two weeks later, differentiated EBs (Figure 2E) were plated onto fibronectin-coated plates. Large quantities of dendritic-like cells with high proliferative ability could be observed thereafter, whereas epithelium-like cells were rarely found (Figure 2F). Single cells were dissociated and passaged at week 3, which usually showed a typical dendritic morphology at weeks 5–6 after differentiation (Figure 2G). High proliferative activity was maintained even after several rounds of freezing and thawing. In addition, the pigmentation of the cell pellet gradually darkened throughout culture, which also usually became remarkable by weeks 5–6 (Figure 2H). Thus, hiMels were successfully generated using this suspensive system and the same protocol was validated with multiple iPSC lines from other vitiligo patients and healthy individuals (Figure S3).

To test whether this differentiation system was superior to the conventional system, the gene expression levels of melanocytic stem and/or progenitor markers were detected. By the end of week 2 of the differentiation process, the levels of *PAX3*, *MITF*, and *SOX10* were 8, 3, and 18 times higher in this system than those in the 2D culture, respectively ($p < 0.05$; Figure 2I; Table S1). Additionally, the percentage of immunostained $PAX3^+$ cells, a marker of melanocyte stem and/or progenitor cells, was calculated as an index of the differentiation efficiency (Figure 2J). In the 3D system, the percentage was approximately double that

(F) Teratoma formation assay: respiratory epithelium (endoderm), cartilage (mesoderm), and pigment (ectoderm) cells found in a representative teratoma induced by injection of a clone of JSDV-5 cells into the testis of a non-obese diabetic severe combined immunodeficiency (NOD-SCID) mouse.
(G) Bisulfite genomic sequencing of the promoter regions of *OCT4*. Open and closed circles indicate demethylated and methylated CpG site (CpGs; clone JSDV-5).
(H) Chromosome analysis (clone JSDV-5). Results are representative of at least three independent experiments.
Scale bars: 200 μm (A–C) and 100 μm (E and F). See also Figure S1.

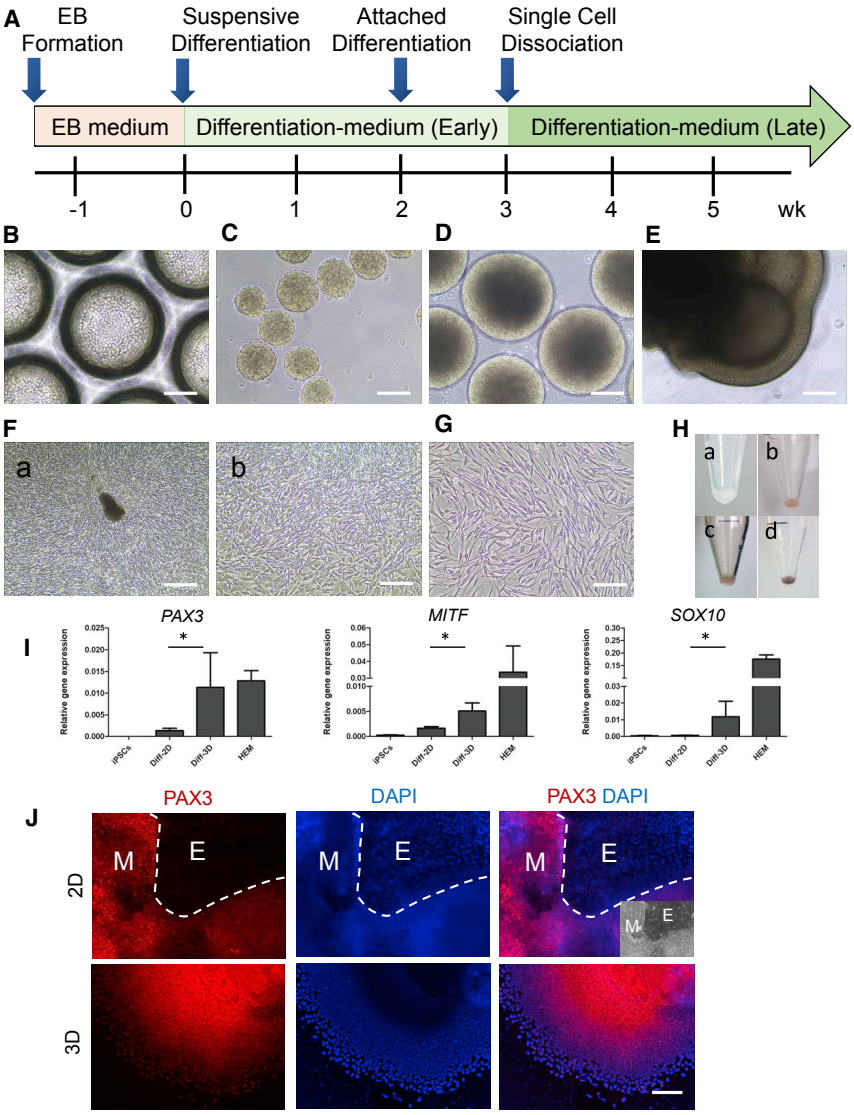

Figure 2. Suspension Culture for Differentiation into iMelanocytes

(A) Flow chart of suspensive differentiation.

(B) Single-cell suspension of iPSCs on Elplasia plates.

(C) Embryoid bodies (EBs) cultured at day 1.

(D) EBs cultured at day 10.

(E) Differentiated EBs in the suspension system at week 2.

(F) Large number of dendritic-like cells in the peripheral area of EBs on fibronectin-coated plates at week 3.

(G) Split cells displayed the typical morphology of melanocytes at week 5.

(H) Pigmentation of cell pellets at weeks 0 (a), 3 (b), 4 (c), and 5 (d), respectively.

(I) Comparison of gene expression of *PAX3*, *MITF*, and *SOX10* in the 2D and 3D culture systems at week 2 of differentiation. Bars represent the relative quantity normalized to that of *GAPDH* (mean ± SD) calculated from five independent experiments. Asterisks indicate statistically significant differences (*$p < 0.05$, Student's t tests).

(J) Immunostaining of differentiated EBs with PAX3 in the 2D and 3D systems (after attachment on fibronectin-coated dishes) at week 2.

E, epithelial-like cells; M, iMelanocytes. Results are representative of at least three independent experiments. Scale bar: 200 μm. See also Figures S2 and S3 and Table S1.

detected in the 2D culture condition (79.5% ± 13.7% versus 38.1% ± 12.6%, $p < 0.001$; Table S1). Overall, these results suggest that this 3D suspensive system considerably improved the efficiency of the generation of iPSC-derived hiMels.

In Vitro Characteristics of Patient iMels

To investigate whether the patient iMels exhibited the characteristics of normal human epidermal melanocytes (HEMs), we detected the expression levels of melanocytic marker genes such as *MITF*, *PAX3*, *SOX10*, *KIT*, *TYR*, *TYRP1*, and *DCT*, which were found to be highly expressed in patient iMels with levels equivalent to those of iMels derived from healthy iPSCs and HEMs (Figure 3A). Exogenous genes were not detectable (Figure 3B). Patient iMels were also immunocytochemically positive for TYRP1, TYR, and MITF (Figure 3C), and exhibited positive results in L-DOPA (Figure 3D) and Masson-Fontana (Figure 3E) staining. In addition, we confirmed the generation of melanosomes, which are required for the production of melanin, in the cytoplasm of patient iMels using transmission electron microscopy, and found that these organelles were present at a level similar to that of the positive control, HEMs (Figure 3F). To further assess whether there are stem and/or progenitor cells existing in the pool of hiMels, the expression of stem and/or progenitor cell markers was detected, which showed that *PAX3*, *MITF*, and *SOX10* were expressed as early as the first week (Figures S2D and S2E) and their levels increased steadily in the process of differentiation (Figure S2D). When hiMels became fully mature at week 7, their expression levels of *PAX3* and *MITF* were still much higher than those in HEMs (Figure S2D). Taken together, these data demonstrate that patient iPSCs could differentiate into functional melanocytes that share *in vitro* characteristics and functions with HEMs and express higher levels of stem and/or progenitor cell-related genes than HEMs.

Transcriptome Characteristics Based on RNA Sequencing

Next, to better understand the genetic basis of vitiligo, we performed RNA sequencing with iPSCs, hiMels, and HEMs. Analysis of differentially expressed genes between melanocytes and iPSCs indicated that patient iMels showed similar transcriptome characteristics to HEMs (Figure 4A) and their melanocytic genes were comparably expressed (Figure 4B). There were 7,745 genes commonly expressed between these two types of melanocytes, which accounted for 93.3% of the genes reliably

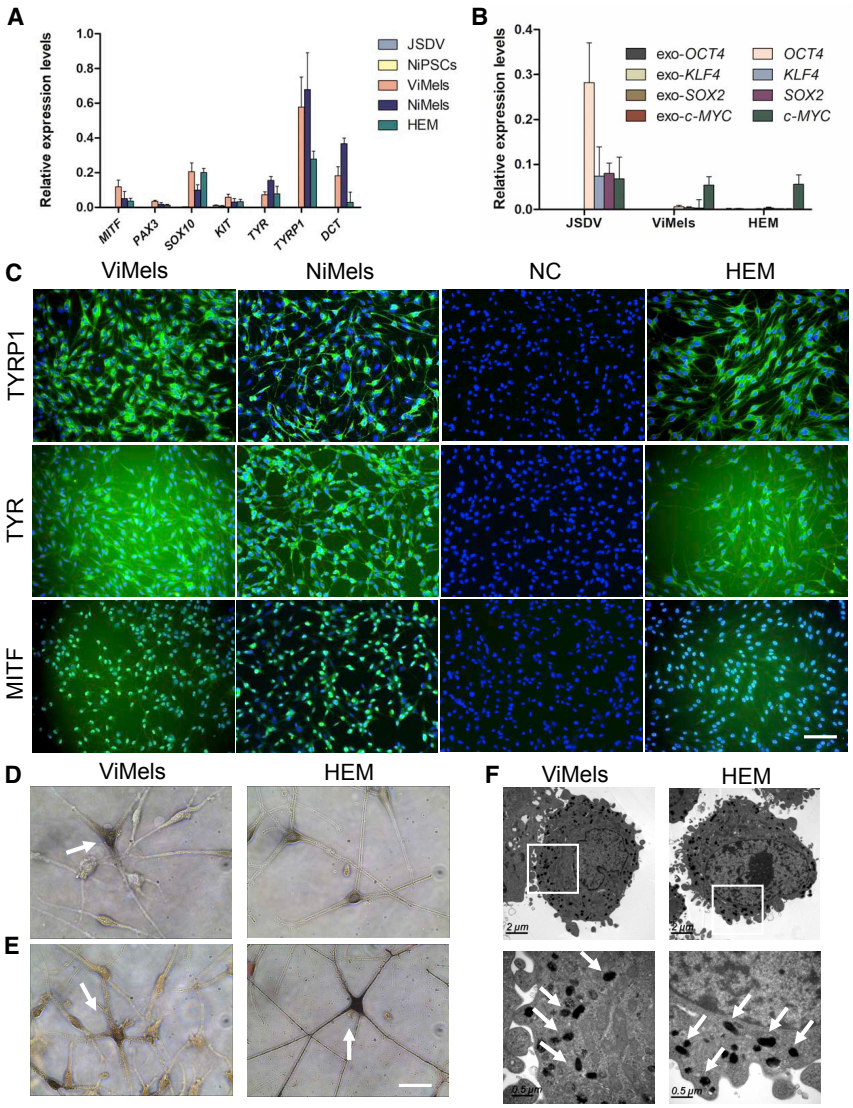

Figure 3. Characterization of iMelanocytes *In Vitro*

(A) qPCR analysis showed that ViMels (patient iPSC-derived melanocytes) and NiMels (healthy iPSC-derived melanocytes) expressed melanocytic marker genes at levels comparable to those of normal HEMs. Bars represent the relative quantity normalized to *GAPDH* (mean ± SD), calculated from four independent experiments.

(B) qPCR analysis showing that the exogenous Yamanaka factors were silenced in both JSDV cells and ViMels, whereas *c-MYC* was expressed at low levels in both ViMels and HEMs.

(C) Immunostaining analysis of ViMels and NiMels using antibodies against melanocyte-specific proteins. NC, negative control.

(D) Positive L-DOPA staining of ViMels.

(E) Masson-Fontana staining of ViMels.

(F) Transmission electron microscopy image of mature melanosomes (arrows) in the cytoplasm of ViMels. Results are representative of at least three independent experiments.

Scale bar: 200 μm (C) and 50 μm (D and E). See also Figure S2.

detected in HEMs (Figure 4C). Moreover, the gene expression levels were highly correlated between patient iMels and HEMs ($r = 0.91$) and genes involved in melanogenesis such as *MITF*, *SOX10*, *DCT*, *PEML*, *TYRP1*, and *TYR* were significantly upregulated in patient iMels (Figure 4D).

To assess the differences between patient iMels and HEMs and explore significant pathways related to vitiligo, their differentially expressed genes were analyzed through Ingenuity Pathway Analysis (IPA). The results demonstrated the involvement of multiple canonical signaling pathways (Table 1). Interestingly, we found some classic pathways that accorded with reported mechanisms of vitiligo, such as interferon (IFN) signaling (Figure S4) (Bertolotti et al., 2014; Briggs et al., 2011; Yang et al., 2015). Greater susceptibility to oxidative stress has been reported in melanocytes from patients with vitiligo compared to those from unaffected individuals, which contributes to melanocyte damage in vitiligo (Jimbow et al., 2001; Maresca et al., 1997). We also identified multiple pathways linked with the oxidative stress response in melanocytes, including oxidative phosphorylation (Sahoo et al., 2017; Spiegelman and Elcheva, 2017), PI3K-AKT signaling (Kim et al., 2017; Shin et al., 2014), and NRF-2 (Shin et al., 2014). Therefore, the RNA sequencing data not only indicate the high similarity in transcriptome characteristics between patient iMels and HEMs but also reveal multiple signaling pathways involved in the pathogenesis of vitiligo.

Reconstitution of Pigmented Hair Follicles *In Vivo*

To confirm the *in vivo* functions of hiMels, we adopted a modified hair follicle reconstitution assay (Figure S5A) (Yang et al., 2014). In brief, patient iMels were injected into the back skin of nude mice, which were mixed with epidermal aggregates and dermal fibroblasts isolated from the skin of neonatal BALB/c mice. HEMs and human dermal fibroblasts were used as controls instead of hiMels. Two weeks later, the grafts were harvested (Figure S5B) and pigmented hair follicles were found in mice transplanted with patient iMels and HEMs (Figures 5A and S5C), whereas white hairs were generated in animals transplanted with fibroblasts (Figure S5D). In the reconstituted tissue with hiMels, L-DOPA-positive melanocytes were found in the hair bulb and epidermis (Figures 5B, S5E, and S5G). Masson-Fontana staining, which reveals the pattern of melanin distribution, showed that pigmentation was mainly localized in the hair bulb, hair shafts, as well as in the reconstituted epidermis (Figures 5C, S5F, and S5H). By contrast, massive melanin was deposited in the surrounding connective tissue after transplantation with HEMs, whereas only quite limited melanin was located in the hair bulb (Figure S5I). Immunostaining showed

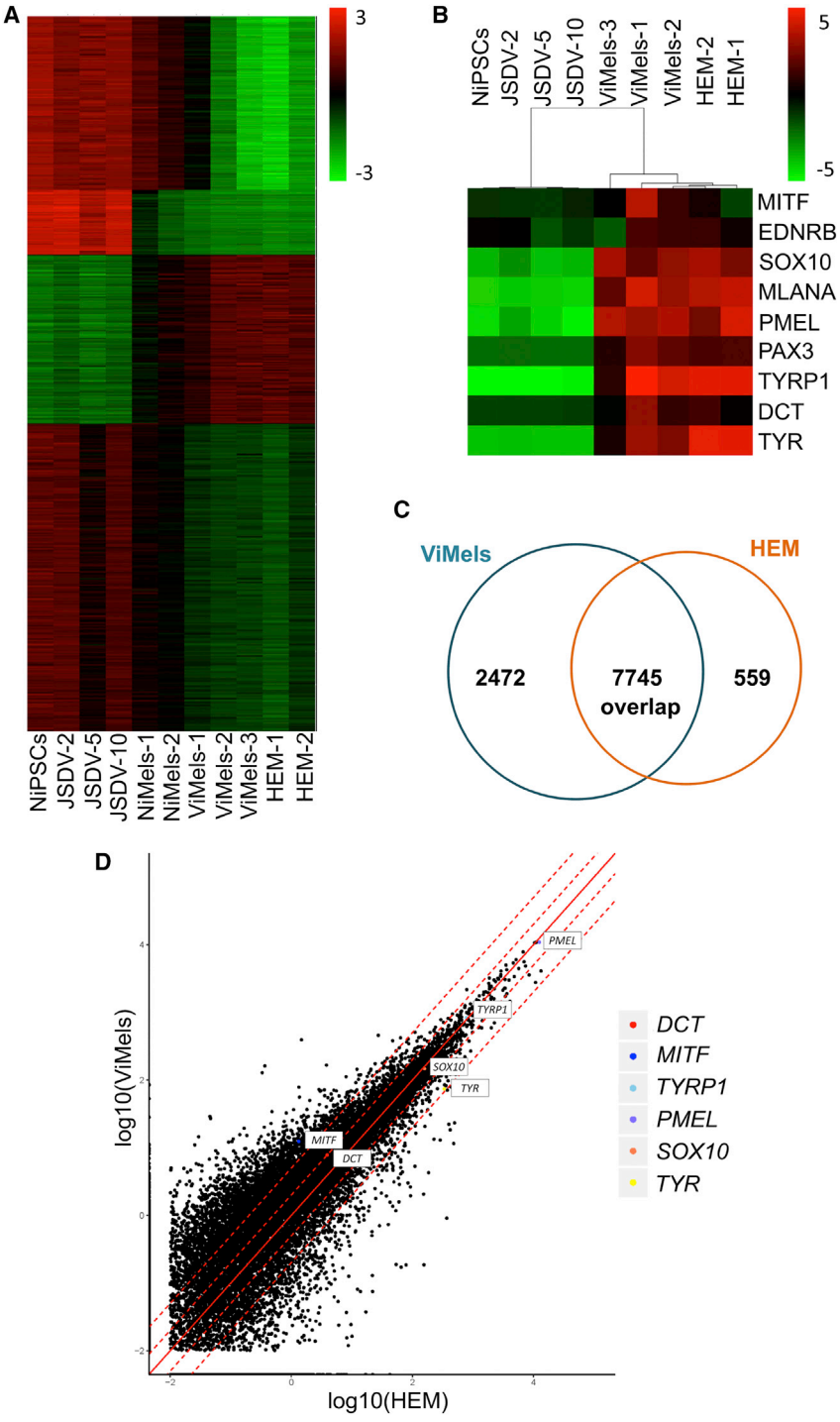

Figure 4. Molecular Similarity of iMelanocytes and Human Epidermal Melanocytes

(A) Heatmap of genes differentially expressed in JSDV cells (patient iPSCs), NiPSCs, ViMels, NiMels, and HEMs (HEM-1, neonatal; HEM-2, adult) according to RNA sequencing (RNA-seq) analysis.

(B) Heatmap of genes involved in the differentiation of melanocytes.

(C) Venn diagram showing that of the 8,304 reliably detected genes in HEMs, 7,745 were also expressed in ViMels.

(D) Scatterplots showing a high correlation of gene expression levels in HEMs and ViMels (r = 0.91). Melanocytic markers are indicated by colored circles. See also Figure S4.

that the hiMels localized in the hair blub and basal cell layer of the reconstituted epidermis expressed the melanocytic markers MITF, PAX3, and TYRP1 (Figures 5D, 5E, 5F, and S5J). To further verify that these melanin-producing cells were human derived, we used a specific antibody recognizing the human nucleus antigen and found that the positive cells also expressed TYRP1 (Figures 5G and S5K). Thus, these results reveal that mature hiMels could integrate into the hair bulb and epidermis of the reconstituted skin and produce melanin.

Maintenance of Long-Term Function

Since the hiMels were shown to express the melanocytic stem and/or progenitor markers MITF and PAX3 *in vivo*, we next evaluated whether these stem and/or progenitor cells could integrate into the hair bulge of the grafts and provide long-term function maintenance. Indeed, cells co-expressing MITF and PAX3 were not only localized in the hair blub but also in the bulge-subbulge region, which was positive for the hair follicle stem cell marker KRT15 (Figure S6A). These human-origin cells in the bulge area were negative for TYRP1 expression (Figure 6A), suggesting a stem and/or progenitor feature. Another hair follicle stem cell marker, ITGA6, was also successfully used to localize these $MITF^{+}TYRP1^{-}$ hiMels not only in the anagen hair follicle (Figures 6B and S6B) but also in catagen or telogen follicles (Figure 6C). To confirm whether these stem and/or progenitor hiMels contribute to long-term function maintenance, we modified and established another hair follicle reconstitution assay using a chamber (Figure S6C) (Lichti et al., 2008). In this revised model, newly formed hairs grew outward (Figure S6D) and properly shed in the telogen phase, which did not occur in the previous model established through hypodermal injection. Additionally, since the host mice (BALB/c Nude) still have partial immunity, which is even strengthened as they age during the longer observation period, it is not suitable for the long-term survival of hiMels. Therefore, we used an anti-Asialo GM1 antibody which depletes natural killer cells and a subset of monocyte and macrophages *in vivo* (Habu et al., 1981; Kasai et al., 1980). With this method, patient iMels were still clearly detectable in the anagen hair

Table 1. Patient iMels Associated Canonical Signaling Pathways

Pathways	-log(p Value)	Overlap with Dataset (%)
Cell cycle: G2/M DNA damage checkpoint regulation	5.47	26/48 (54.2)
Oxidative phosphorylation	5.32	42/95 (44.2)
Phagosome maturation	5.31	51/123 (41.5)
Mitochondrial dysfunction	4.5	57/150 (38.0)
PI3K-AKT signaling	3.89	47/123 (38.2)
Cyclins and cell cycle regulation	3.71	32/76 (42.1)
Interferon signaling	3.48	16/30 (53.3)
NRF2-mediated oxidative stress response	3.09	61/181 (33.7)
Cell cycle control of chromosomal replication	2.9	22/51 (43.1)
Retinoic acid mediated apoptosis signaling	2.72	19/43 (44.2)
Antigen presentation pathway	2.56	15/32 (46.9)
mTOR signaling	1.96	59/193 (30.6)
Semaphorin signaling in neurons	1.47	16/44 (36.4)
UVA-induced MAPK signaling	1.4	31/99 (31.3)
Integrin signaling	1.37	55/191 (28.8)

See also Figure S4.

follicles at week 7 after transplantation (Figures 6D, 6E, S6E, and S6F) and the pigmentation was localized in the epidermis, hair bulb, and hair shafts (Figure 6F). These results indicate that the stem and/or progenitor hiMels in the hair bulge could provide long-term maintenance even after a hair growth cycle.

Collectively, these results demonstrate that patient iMels were functional *in vivo* and contributed to the reconstitution of the hair follicle and epidermis. Mature hiMels integrated into the hair bulb and basal cell layer and took part in the generation of pigmented hair shafts and the epidermis. Meanwhile, the existing hair follicle stem cells in the bulge region function as a niche for melanocyte stem cells and should support and provide the long-term function maintenance of hiMels.

DISCUSSION

A 3D suspensive culture system has been shown to provide a more appropriate niche environment and to better mimic the natural cellular organization and function *in vivo* than conventional 2D culture and has, thus, been widely applied for iPSCs differentiation and organoid generation (Haraguchi et al., 2015; Jo et al., 2016; Lancaster et al., 2013; Lee et al., 2018; Muguruma et al., 2015; Paşca et al., 2015). In this study, we established a suspensive system for the generation of iPSC-derived hiMels, which reduced the percentage of epithelium-like cells and significantly improved the differentiation efficiency compared to the conventional method. These improved effects are considered to be related to the better proliferative capability of hiMels in a 3D suspensive system, which inhibited the growth of epithelium-like cells. Moreover, since epithelium-like cells in a flat culture condition proliferate quickly, which requires more flat spaces to be available, usually no more than 10 EBs can be implanted per well on a six-well plate at the beginning of differentiation. By contrast, we were able to implant double the number of EBs in the same cultural unit using the suspensive system (Table S1).

It has long been difficult to evaluate the *in vivo* function of human melanocytes because the xeno microenvironment is inappropriate for the survival of these cells. Recently, Kawakami et al. (2018) transplanted human iPSC-derived melanocytes into the skin regions. However, these cells were not localized in the normal sites for mature melanocytes, and the observation duration was quite limited. Here, we adopted and modified a hair follicle reconstitution assay (Yang et al., 2014) to create a better microenvironment for the survival of hiMels, and successfully reconstituted pigmented hair follicles and epidermis. In the grafts, mature hiMels were localized in the hair bulb and basal cell layer, the normal sites for mature melanocytes in humans (Tobin, 2011). Moreover, Masson-Fontana staining indicated that melanin was also distributed in the hair shafts, indicating the melanin transportation from hiMels to mouse keratinocytes.

Follicular pigmentation is considered to be a result of structural and functional interactions involving melanocytes, matrix keratinocytes, and dermal papilla fibroblasts (Cichorek et al., 2013). The process of hair pigmentation also involves the melanogenic activity of follicular melanocytes, transfer of melanin granules into keratinocytes, and formation of pigmented hair shafts (Slominski et al., 2005). Thus, this work suggests that mature hiMels can interact with mouse cells, produce and transfer melanin to the surrounding keratinocytes, and eventually generate pigmented hair follicles and hair shafts.

However, the initial hair follicles reconstituted in the grafts will undergo a growth cycle and these mature hiMels will turnover with time. If there are stem and/or progenitor cells existing in the pool of hiMels, they would allow for the sustainable regeneration of melanin in new hair cycles. As expected, human-derived $MITF^{+}PAX3^{+}TYRP1^{-}$ stem and/or progenitors iMels were co-localized with hair follicle stem cells (marked with KRT15 and ITGA6) in the bulge-subbulge region, in line with the results of previous studies (Gleason et al., 2008; Nishimura, 2011; Nishimura et al., 2005; Osawa et al., 2005). At week 7 after transplantation, mature hiMels were still clearly detectable in the bulb of anagen hairs (identified by immunostaining, DOPA, and Masson-Fontana staining). Thus, these results demonstrate that hair follicle stem cells localized in the bulge region provide a functional niche for melanocyte stem cells (Tanimura et al., 2011). To the best of our knowledge, these data demonstrate the longest survival and function maintenance of iPSC-derived melanocytes *in vivo*, confirming their hair follicle and epidermis reconstitution capacity. Moreover, this work represents the best record involving xenografts of human melanocyte transplantation into nude mice.

For humans, melanocytes in the hair follicles share many common characteristics with those in the epidermis, and they are closely linked with each other. The process of melanin transport from follicular melanocytes to the neighboring keratinocytes in the growing hair shaft is similar to the epidermal phagocytosis of melanosomes in keratinocytes (Cichorek et al., 2013). Additionally, the most common presentation of repigmentation in vitiligo after treatment is a perifollicular pattern, which is mainly dependent on follicular melanocytes (Birlea et al., 2017).

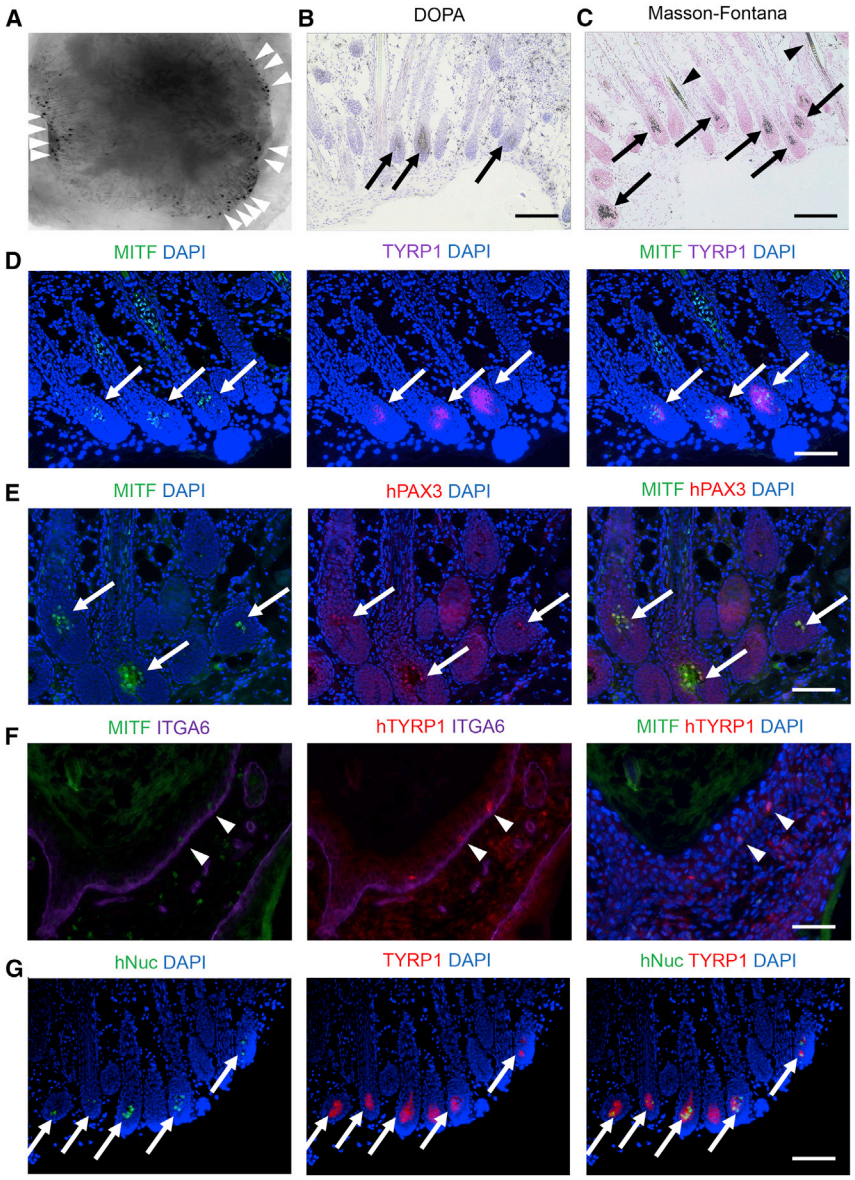

Figure 5. Reconstitution of Pigmented Hair Follicles with Patient iMelanocytes *In Vivo*

(A) Pigmented hair follicles (arrowheads) were formed in nude mice injected with patient iMels.

(B) Patient iMels (arrows) were mainly localized in the hair bulb as shown by L-DOPA staining.

(C) Distribution of melanin in the hair bulb and hair shafts as shown by Masson-Fontana staining. Arrows, melanin in the hair bulb; arrowheads, melanin in the hair shafts.

(D) Immunostaining of reconstituted hair follicles with melanocytic markers, MITF (green) and TYRP1 (purple). Arrows: $MITF^{+}TYRP1^{+}$ cells in the hair bulb.

(E) Immunostaining of reconstituted hair follicles with melanocytic markers, MITF (green) and hPAX3 (red). Arrows: $MITF^{+}hPAX3^{+}$ cells in the hair bulb.

(F) Immunostaining showing that cells expressing MITF (green) and hTYRP1 (red) were co-localized with the basal cell layer, marked with ITGA6 (purple).

(G) Immunofluorescence staining showing the co-localization of signals from antibodies recognizing human nuclei (hNuc, green) and the melanocytic marker TYRP1 (red) in the hair bulb. Results are representative of at least three independent experiments.

Scale bars: 200 μm (B, C, and G), 100 μm (D and E), and 50 μm (F). See also Figure S5.

Therefore, the model developed in our study provides a tool to reveal the potential functions of hiMels after transplantation.

Interestingly, we also found that the integration efficiency of patient iMels into mouse hair follicles was higher than that of HEMs according to multiple experiments in different individuals. Melanin produced by hiMels was mainly localized in the hair bulb and hair shafts, whereas massive melanin deposits were detected in the connective tissue around the hair follicles after HEM injection, indicating that most of the HEMs failed to survive in the grafts. The different outcome after transplantation of hiMels and HEMs might be associated with two key factors that are tightly coordinated: proliferation and differentiation. Premature differentiation can result in a depletion of proliferating cells and organ failure (Lee et al., 2013). In our study, we typically transplanted hiMels at about week 5 of differentiation, which maintained a high level of proliferative activity but were not as mature as the HEMs (the color of the cell pellet was usually dark gray and not as black as that of the HEM pellet). By contrast, the HEMs used in our study were fully mature and their proliferative ability decreased gradually with the duration of culture. Thus, our results support the importance of maintaining the balance between proliferation and differentiation for organ formation and tissue maintenance, which is especially critical in tissues that undergo rapid turnover such as the skin (Lee et al., 2013). Additionally, we found a considerable number of hiMels that were DOPA positive but Masson-Fontana negative (Figures S5G and S5H) or showed MITF-positive but TYRP1 negative (Figures 6B and 6C) in the dermis, suggesting that hiMels are heterogeneous populations with different degrees of maturation and that stem and/or progenitor cells might contribute to the progression of hiMels *in vivo*.

Vitiligo is featured by the loss of functional melanocytes, and various hypotheses have been suggested to explain this loss. With the availability of patient iPSC-derived iMels, the melanogenic process and melanocyte development *ex vivo* may serve as a model to discover the intrinsic mechanism of melanocyte loss-related diseases. Although this model will not resolve all of the current challenges in understanding the complete mechanism, the first signs of the dawn are beginning to appear.

There are several vitiligo-related signal pathways and networks, which accord with the hypotheses of mechanisms proposed during the past few decades in this field. Gaining a

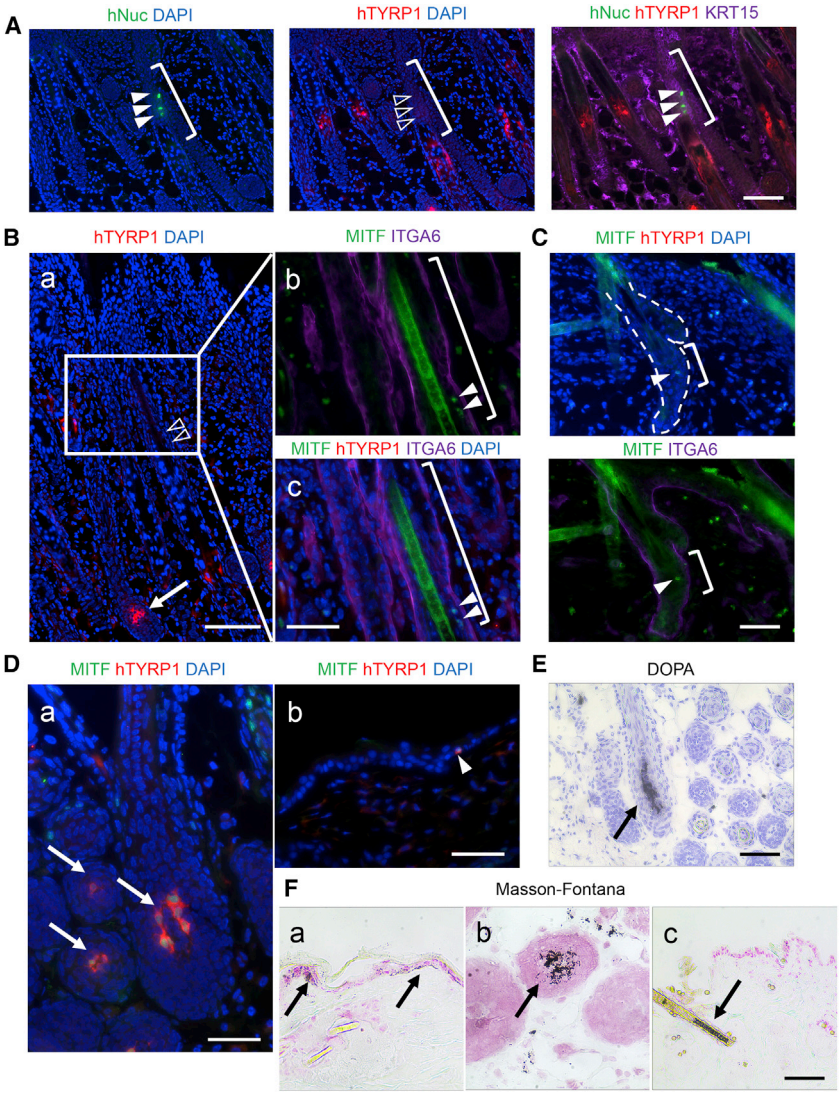

Figure 6. Maintenance of the Long-Term Function of iMelanocytes *In Vivo*

(A–C) Reconstituted tissue collected at week 2 after transplantation.

(A) Immunostaining of hair follicles with the human nuclei markers (hNuc, green), hTYRP1 (red), and hair follicle stem cell marker KRT15 (purple). The bulge areas are demarcated by brackets. Arrowheads: $hNuc^{+}/hTYRP1^{-}$ cells in the bulge area of an anagen hair follicle.

(B) Immunostaining of hair follicles with the melanocytic markers MITF (green), hTYRP1 (red), and hair follicle stem cell marker ITGA6 (purple). The bulge areas are demarcated by brackets. Arrow, $hTYRP1^{+}$ cells in the hair bulb; arrowheads, $MITF^{+}/hTYRP1^{-}$ cells in the bulge region of an anagen hair follicle.

(C) Immunostaining showing $MITF^{+}/hTYRP1^{-}$ cells co-localized with ITGA6 in the bulge region of a catagen or telogen hair follicle.

(D–F) Reconstituted tissue collected at week 7 after transplantation.

(D) Immunostaining of reconstituted tissue after transplantation with MITF (green) and hTYRP1 (red). (a) Arrows, $MITF^{+}/hTYRP1^{+}$ cells in the hair bulb; (b) arrowhead, $MITF^{+}/hTYRP1^{+}$ cells in the epidermis.

(E) hiMels were localized in an anagen hair bulb as determined by L-DOPA staining.

(F) Distribution of melanin in the reconstituted epidermis (a), hair bulb (b), and hair shafts (c) determined by Masson-Fontana staining. Results are representative of at least three independent experiments.

Scale bars: 100 μm (A, Ba, E, Fa, and Fc) and 50 μm (Bb, Bc, C, D, and Fb). See also Figure S6.

comprehensive understanding and integration of these hypotheses will undoubtedly lead to new concepts and treatment solutions. The association between IFN and melanocytes as well as vitiligo has been reported upon in a large number of studies. IFN-γ showed strong adverse effects on cultured human melanocytes, such as melanogenesis inhibition, viability loss, apoptosis, cell cycle arrest, and senescence (Wang et al., 2014; Yang et al., 2015). Moreover, the development of vitiligo has been reported in some patients after treatment with IFN therapy for primary diseases such as viral hepatitis (Anbar et al., 2008; Hamadah et al., 2010), melanoma (Daneshpazhooh et al., 2006; Gogas et al., 2006; Richards et al., 1992), and multiple sclerosis (Coghe et al., 2018; Kocer et al., 2009). However, there is also direct evidence of this association based on the abnormal expression of IFN in patients with vitiligo. The mRNA and protein expression levels of IFN-γ or type I IFN were shown to be increased in the blood samples of patients with active vitiligo compared with those of patients with stable disease or healthy controls (Briggs et al., 2011; Dwivedi et al., 2013). The IFN-specific signature or IFN-producing cells were also elevated in the blood or skin lesions (Abdallah et al., 2018; Badri et al., 1993; Bertolotti et al., 2014; Rashighi et al., 2014; Yang et al., 2015). Overall, there appears to be a strong association between IFN and melanocytes destruction as well as vitiligo development. In the present study, RNA sequencing also showed the involvement of IFN signaling pathway and upregulation of IFN-γ receptors in patient iMels. Combined with other IPA results, we assumed that the abnormal response of patient melanocytes to IFN (due to upregulation of the receptor) and/or to oxidative stress leads to the autoimmune-mediated melanocyte destruction and vitiligo progression (Richmond et al., 2013). However, given the limited sample size and the fact that the same mechanisms might not apply to all cases, the involvement of these pathways in the pathogenesis of vitiligo will need to be verified with larger samples in an effort toward identifying target molecules for therapy.

There is particular concern for the safety of transplanted donor cells for their clinical application. In our experiments, patient iMels without exogenous genes ultimately underwent senescence after continued culturing for several months. Tumorigenicity was also not found in the grafts at week 7 after transplantation (tumors are usually detectable at week 2 or 3 after transplantation of

melanoma cell lines in nude mice; data not shown). These results indicated a lack of tumorigenicity of iPSC-derived melanocytes, which will pave the way for their potential clinical application in cellular transplantation therapy. Nevertheless, modified protocols for generating clinical-grade melanocytes are necessary, and the lack of tumorigenicity must also be confirmed in more stringent experiments in the future. Recently, autologous transplantation of iPSC-derived retinal pigment epithelial cells was performed, with no serious adverse event noted (Mandai et al., 2017). Melanocytes and retinal pigment epithelial cells share many common aspects, including their embryonic origin. Therefore, this clinical study provides important information regarding the possibility of iPSC-derived melanocytes in autologous transplantation therapy.

In conclusion, we demonstrated that iPSCs of vitiligo patients have the potential to differentiate into melanocytes, with functionality observed both *in vitro* and *in vivo*. More significantly, these hiMels possessed capacities of hair follicle and epidermis reconstitution and long-term function maintenance. Thus, our work provides a potential resource of cells for personalized cellular therapy of patients with depigmentation. In addition, our findings may provide insight into the pathogenesis of vitiligo.

STAR★METHODS

Detailed methods are provided in the online version of this paper and include the following:

- KEY RESOURCES TABLE
- CONTACT FOR REAGENT AND RESOURCE SHARING
- EXPERIMENTAL MODEL AND SUBJECT DETAILS
  - Information of Patients with Vitiligo
  - Fibroblasts of Patients
  - Patient iPSC Lines
  - Animal Studies
- METHOD DETAILS
  - Teratoma Formation
  - Uniform Embryoid Body Formation
  - Conventional Differentiation System
  - Suspension Differentiation System
  - Hair Follicle Reconstitution Assay
  - Real-time PCR
  - RNA Sequencing
  - Bioinformatics for RNA Sequencing Data
  - Immunocytochemistry
  - $_{L}$-DOPA Staining
  - Masson-Fontana Staining
- QUANTIFICATION AND STATISTICAL ANALYSIS
- DATA AND SOFTWARE AVAILABILITY

SUPPLEMENTAL INFORMATION

Supplemental Information can be found online at https://doi.org/10.1016/j.celrep.2019.03.046.

ACKNOWLEDGMENTS

We thank Dr. Jaejeong Kim of the University of Tsukuba Faculty of Medicine for designing the graphical abstract. This research was supported partly by the National Natural Science Foundation of China (81770621 to Y.-W.Z.), a grant from the National Natural Science Foundation of China (81573053 to Y.-M.L.), the Ministry of Education, Culture, Sports, Science, and Technology of Japan, KAKENHI (16K15604 and 18H02866 to Y.-W.Z.), and the Natural Science Foundation of Jiangsu Province (BK20180281 to L.-P.L.).

AUTHOR CONTRIBUTIONS

Conceptualization, Y.-W.Z., Y.-M.L., and L.-P.L.; Methodology, Y.-W.Z., L.-P.L., and Y.G.; Specimen Collection, H.X.; Experiments, L.-P.L., N.-N.G., S.L., Y.-X.Z., Y.G., J.-L.H., and L.-Y.W.; Formal Analysis, L.-P.L. and N.-N.G.; Bioinformatics, X.-L.M. and D.-X.Z.; Resources, Y.-M.L., L.H., and Y.-W.Z.; Writing, L.-P.L.; Manuscript Reviewing and Rewriting, Y.-W.Z. and L.-P.L.; and Funding Acquisition, Y.-W.Z., Y.-M.L., and L.-P.L.

DECLARATION OF INTERESTS

L.-P.L. has a patent pending for a suspension system of iPSC-derived melanocytes differentiation (201810419157.6, China).

Received: May 6, 2018
Revised: February 2, 2019
Accepted: March 13, 2019
Published: April 9, 2019

REFERENCES

Abdallah, M., El-Mofty, M., Anbar, T., Rasheed, H., Esmat, S., Al-Tawdy, A., Fawzy, M.M., Abdel-Halim, D., Hegazy, R., Gawdat, H., et al.; Egyptian Vitiligo Group (2018). CXCL-10 and Interleukin-6 are reliable serum markers for vitiligo activity: A multicenter cross-sectional study. Pigment Cell Melanoma Res. *31*, 330–336.

Anbar, T.S., Abdel-Rahman, A.T., and Ahmad, H.M. (2008). Vitiligo occurring at site of interferon-alpha 2b injection in a patient with chronic viral hepatitis C: a case report. Clin. Exp. Dermatol. *33*, 503.

Badri, A.M., Todd, P.M., Garioch, J.J., Gudgeon, J.E., Stewart, D.G., and Goudie, R.B. (1993). An immunohistological study of cutaneous lymphocytes in vitiligo. J. Pathol. *170*, 149–155.

Barman, K.D., Khaitan, B.K., and Verma, K.K. (2004). A comparative study of punch grafting followed by topical corticosteroid versus punch grafting followed by PUVA therapy in stable vitiligo. Dermatol. Surg. *30*, 49–53.

Bertolotti, A., Boniface, K., Vergier, B., Mossalayi, D., Taieb, A., Ezzedine, K., and Seneschal, J. (2014). Type I interferon signature in the initiation of the immune response in vitiligo. Pigment Cell Melanoma Res. *27*, 398–407.

Birlea, S.A., Goldstein, N.B., and Norris, D.A. (2017). Repigmentation through melanocyte regeneration in vitiligo. Dermatol. Clin. *35*, 205–218.

Briggs, T.A., Rice, G.I., Daly, S., Urquhart, J., Gornall, H., Bader-Meunier, B., Baskar, K., Baskar, S., Baudouin, V., Beresford, M.W., et al. (2011). Tartrate-resistant acid phosphatase deficiency causes a bone dysplasia with autoimmunity and a type I interferon expression signature. Nat. Genet. *43*, 127–131.

Cichorek, M., Wachulska, M., Stasiewicz, A., and Tymińska, A. (2013). Skin melanocytes: biology and development. Postepy Dermatol. Alergol. *30*, 30–41.

Coghe, G., Atzori, L., Frau, J., Fenu, G., Lorefice, L., Marrosu, M.G., and Cocco, E. (2018). Localized pigmentation disorder after subcutaneous pegylated interferon beta-1a injection. Mult. Scler. *24*, 231–233.

Cook, A.L., Smith, A.G., Smit, D.J., Leonard, J.H., and Sturm, R.A. (2005). Co-expression of SOX9 and SOX10 during melanocytic differentiation in vitro. Exp. Cell Res. *308*, 222–235.

Daneshpazhooh, M., Shokoohi, A., Dadban, A., and Raafat, J. (2006). The course of melanoma-associated vitiligo: report of a case. Melanoma Res. *16*, 371–373.

Dwivedi, M., Laddha, N.C., Shah, K., Shah, B.J., and Begum, R. (2013). Involvement of interferon-gamma genetic variants and intercellular adhesion

molecule-1 in onset and progression of generalized vitiligo. J. Interferon Cytokine Res. *33*, 646–659.

Eisen, M.B., Spellman, P.T., Brown, P.O., and Botstein, D. (1998). Cluster analysis and display of genome-wide expression patterns. Proc. Natl. Acad. Sci. USA *95*, 14863–14868.

Ezzedine, K., Eleftheriadou, V., Whitton, M., and van Geel, N. (2015). Vitiligo. Lancet *386*, 74–84.

Fang, D., Leishear, K., Nguyen, T.K., Finko, R., Cai, K., Fukunaga, M., Li, L., Brafford, P.A., Kulp, A.N., Xu, X., et al. (2006). Defining the conditions for the generation of melanocytes from human embryonic stem cells. Stem Cells *24*, 1668–1677.

Fehrenbach, S., Novak, D., Bernhardt, M., Larribere, L., Boukamp, P., Umansky, V., and Utikal, J. (2016). Loss of tumorigenic potential upon transdifferentiation from keratinocytic into melanocytic lineage. Sci. Rep. *6*, 28891.

Gleason, B.C., Crum, C.P., and Murphy, G.F. (2008). Expression patterns of MITF during human cutaneous embryogenesis: evidence for bulge epithelial expression and persistence of dermal melanoblasts. J. Cutan. Pathol. *35*, 615–622.

Gogas, H., Ioannovich, J., Dafni, U., Stavropoulou-Giokas, C., Frangia, K., Tsoutsos, D., Panagiotou, P., Polyzos, A., Papadopoulos, O., Stratigos, A., et al. (2006). Prognostic significance of autoimmunity during treatment of melanoma with interferon. N. Engl. J. Med. *354*, 709–718.

Goldstein, N.B., Koster, M.I., Hoaglin, L.G., Spoelstra, N.S., Kechris, K.J., Robinson, S.E., Robinson, W.A., Roop, D.R., Norris, D.A., and Birlea, S.A. (2015). Narrow band ultraviolet B treatment for human vitiligo is associated with proliferation, migration, and differentiation of melanocyte precursors. J. Invest. Dermatol. *135*, 2068–2076.

Habu, S., Fukui, H., Shimamura, K., Kasai, M., Nagai, Y., Okumura, K., and Tamaoki, N. (1981). In vivo effects of anti-asialo GM1. I. Reduction of NK activity and enhancement of transplanted tumor growth in nude mice. J. Immunol. *127*, 34–38.

Hamadah, I., Binamer, Y., Sanai, F.M., Abdo, A.A., and Alajlan, A. (2010). Interferon-induced vitiligo in hepatitis C patients: a case series. Int. J. Dermatol. *49*, 829–833.

Haraguchi, Y., Matsuura, K., Shimizu, T., Yamato, M., and Okano, T. (2015). Simple suspension culture system of human iPS cells maintaining their pluripotency for cardiac cell sheet engineering. J. Tissue Eng. Regen. Med. *9*, 1363–1375.

Hedayat, K., Karbakhsh, M., Ghiasi, M., Goodarzi, A., Fakour, Y., Akbari, Z., Ghayoumi, A., and Ghandi, N. (2016). Quality of life in patients with vitiligo: a cross-sectional study based on Vitiligo Quality of Life index (VitiQoL). Health Qual. Life Outcomes *14*, 86.

Jimbow, K., Chen, H., Park, J.S., and Thomas, P.D. (2001). Increased sensitivity of melanocytes to oxidative stress and abnormal expression of tyrosinase-related protein in vitiligo. Br. J. Dermatol. *144*, 55–65.

Jo, J., Xiao, Y., Sun, A.X., Cukuroglu, E., Tran, H.D., Göke, J., Tan, Z.Y., Saw, T.Y., Tan, C.P., Lokman, H., et al. (2016). Midbrain-like organoids from human pluripotent stem cells contain functional dopaminergic and neuromelanin-producing neurons. Cell Stem Cell *19*, 248–257.

Jones, J.C., Sabatini, K., Liao, X., Tran, H.T., Lynch, C.L., Morey, R.E., Glenn-Pratola, V., Boscolo, F.S., Yang, Q., Parast, M.M., et al. (2013). Melanocytes derived from transgene-free human induced pluripotent stem cells. J. Invest. Dermatol. *133*, 2104–2108.

Kasai, M., Iwamori, M., Nagai, Y., Okumura, K., and Tada, T. (1980). A glycolipid on the surface of mouse natural killer cells. Eur. J. Immunol. *10*, 175–180.

Kawakami, T., Okano, T., Takeuchi, S., Osumi, K., Soma, Y., Itoh, M., Hirobe, T., and Jimbow, K. (2018). Approach for the derivation of melanocytes from induced pluripotent stem cells. J. Invest. Dermatol. *138*, 150–158.

Kazantseva, J., Sadam, H., Neuman, T., and Palm, K. (2016). Targeted alternative splicing of TAF4: a new strategy for cell reprogramming. Sci. Rep. *6*, 30852.

Kim, D., Langmead, B., and Salzberg, S.L. (2015). HISAT: a fast spliced aligner with low memory requirements. Nat. Methods *12*, 357–360.

Kim, H., Park, C.S., and Lee, A.Y. (2017). Reduced Nrf2 activation in PI3K phosphorylation-impaired vitiliginous keratinocytes increases susceptibility to ROS-generating chemical-induced apoptosis. Environ. Toxicol. *32*, 2481–2491.

Kocer, B., Nazliel, B., Oztas, M., and Batur, H.Z. (2009). Vitiligo and multiple sclerosis in a patient treated with interferon beta-1a: a case report. Eur. J. Neurol. *16*, e78–e79.

Kumar, A., Mohanty, S., Nandy, S.B., Gupta, S., Khaitan, B.K., Sharma, S., Bhargava, B., and Airan, B. (2016a). Hair & skin derived progenitor cells: In search of a candidate cell for regenerative medicine. Indian J. Med. Res. *143*, 175–183.

Kumar, R., Parsad, D., Rani, S., Bhardwaj, S., and Srivastav, N. (2016b). Glabrous lesional stem cells differentiated into functional melanocytes: new hope for repigmentation. J. Eur. Acad. Dermatol. Venereol. *30*, 1555–1560.

Lancaster, M.A., Renner, M., Martin, C.A., Wenzel, D., Bicknell, L.S., Hurles, M.E., Homfray, T., Penninger, J.M., Jackson, A.P., and Knoblich, J.A. (2013). Cerebral organoids model human brain development and microcephaly. Nature *501*, 373–379.

Lee, J., Böscke, R., Tang, P.C., Hartman, B.H., Heller, S., and Koehler, K.R. (2018). Hair follicle development in mouse pluripotent stem cell-derived skin organoids. Cell Rep. *22*, 242–254.

Lee, S., Kong, Y., and Weatherbee, S.D. (2013). Forward genetics identifies Kdf1/1810019J16Rik as an essential regulator of the proliferation-differentiation decision in epidermal progenitor cells. Dev. Biol. *383*, 201–213.

Li, L., Fukunaga-Kalabis, M., Yu, H., Xu, X., Kong, J., Lee, J.T., and Herlyn, M. (2010). Human dermal stem cells differentiate into functional epidermal melanocytes. J. Cell Sci. *123*, 853–860.

Lichti, U., Anders, J., and Yuspa, S.H. (2008). Isolation and short-term culture of primary keratinocytes, hair follicle populations and dermal cells from newborn mice and keratinocytes from adult mice for in vitro analysis and for grafting to immunodeficient mice. Nat. Protoc. *3*, 799–810.

Lilly, E., Lu, P.D., Borovicka, J.H., Victorson, D., Kwasny, M.J., West, D.P., and Kundu, R.V. (2013). Development and validation of a vitiligo-specific quality-of-life instrument (VitiQoL). J. Am. Acad. Dermatol. *69*, e11–e18.

Linthorst Homan, M.W., Spuls, P.I., Nieuweboer-Krobotova, L., de Korte, J., Sprangers, M.A., Bos, J.D., Wolkerstorfer, A., and van der Veen, J.P. (2012). A randomized comparison of excimer laser versus narrow-band ultraviolet B phototherapy after punch grafting in stable vitiligo patients. J. Eur. Acad. Dermatol. Venereol. *26*, 690–695.

Mandai, M., Watanabe, A., Kurimoto, Y., Hirami, Y., Morinaga, C., Daimon, T., Fujihara, M., Akimaru, H., Sakai, N., Shibata, Y., et al. (2017). Autologous induced stem-cell-derived retinal cells for macular degeneration. N. Engl. J. Med. *376*, 1038–1046.

Maresca, V., Roccella, M., Roccella, F., Camera, E., Del Porto, G., Passi, S., Grammatico, P., and Picardo, M. (1997). Increased sensitivity to peroxidative agents as a possible pathogenic factor of melanocyte damage in vitiligo. J. Invest. Dermatol. *109*, 310–313.

Mort, R.L., Jackson, I.J., and Patton, E.E. (2015). The melanocyte lineage in development and disease. Development *142*, 1387.

Muguruma, K., Nishiyama, A., Kawakami, H., Hashimoto, K., and Sasai, Y. (2015). Self-organization of polarized cerebellar tissue in 3D culture of human pluripotent stem cells. Cell Rep. *10*, 537–550.

Mulekar, S.V., and Isedeh, P. (2013). Surgical interventions for vitiligo: an evidence-based review. Br. J. Dermatol. *169* (*Suppl 3*), 57–66.

Nishimura, E.K. (2011). Melanocyte stem cells: a melanocyte reservoir in hair follicles for hair and skin pigmentation. Pigment Cell Melanoma Res. *24*, 401–410.

Nishimura, E.K., Granter, S.R., and Fisher, D.E. (2005). Mechanisms of hair graying: incomplete melanocyte stem cell maintenance in the niche. Science *307*, 720–724.

Nissan, X., Larribere, L., Saidani, M., Hurbain, I., Delevoye, C., Feteira, J., Lemaitre, G., Peschanski, M., and Baldeschi, C. (2011). Functional melanocytes

derived from human pluripotent stem cells engraft into pluristratified epidermis. Proc. Natl. Acad. Sci. USA *108*, 14861–14866.

Ohta, S., Imaizumi, Y., Okada, Y., Akamatsu, W., Kuwahara, R., Ohyama, M., Amagai, M., Matsuzaki, Y., Yamanaka, S., Okano, H., and Kawakami, Y. (2011). Generation of human melanocytes from induced pluripotent stem cells. PLoS ONE *6*, e16182.

Osawa, M., Egawa, G., Mak, S.S., Moriyama, M., Freter, R., Yonetani, S., Beermann, F., and Nishikawa, S. (2005). Molecular characterization of melanocyte stem cells in their niche. Development *132*, 5589–5599.

Paşca, A.M., Sloan, S.A., Clarke, L.E., Tian, Y., Makinson, C.D., Huber, N., Kim, C.H., Park, J.Y., O'Rourke, N.A., Nguyen, K.D., et al. (2015). Functional cortical neurons and astrocytes from human pluripotent stem cells in 3D culture. Nat. Methods *12*, 671–678.

Pertea, M., Pertea, G.M., Antonescu, C.M., Chang, T.C., Mendell, J.T., and Salzberg, S.L. (2015). StringTie enables improved reconstruction of a transcriptome from RNA-seq reads. Nat. Biotechnol. *33*, 290–295.

Picardo, M., Dell'Anna, M.L., Ezzedine, K., Hamzavi, I., Harris, J.E., Parsad, D., and Taieb, A. (2015). Vitiligo. Nat. Rev. Dis. Primers *1*, 15011.

Rashighi, M., Agarwal, P., Richmond, J.M., Harris, T.H., Dresser, K., Su, M.W., Zhou, Y., Deng, A., Hunter, C.A., Luster, A.D., and Harris, J.E. (2014). CXCL10 is critical for the progression and maintenance of depigmentation in a mouse model of vitiligo. Sci. Transl. Med. *6*, 223ra23.

Richards, J.M., Mehta, N., Ramming, K., and Skosey, P. (1992). Sequential chemoimmunotherapy in the treatment of metastatic melanoma. J. Clin. Oncol. *10*, 1338–1343.

Richmond, J.M., Frisoli, M.L., and Harris, J.E. (2013). Innate immune mechanisms in vitiligo: danger from within. Curr. Opin. Immunol. *25*, 676–682.

Rusfianti, M., and Wirohadidjodjo, Y.W. (2006). Dermatosurgical techniques for repigmentation of vitiligo. Int. J. Dermatol. *45*, 411–417.

Sahoo, A., Lee, B., Boniface, K., Seneschal, J., Sahoo, S.K., Seki, T., Wang, C., Das, S., Han, X., Steppie, M., et al. (2017). MicroRNA-211 regulates oxidative phosphorylation and energy metabolism in human vitiligo. J. Invest. Dermatol. *137*, 1965–1974.

Schneider, M., Dieckmann, C., Rabe, K., Simon, J.C., and Savkovic, V. (2014). Differentiating the stem cell pool of human hair follicle outer root sheath into functional melanocytes. Methods Mol. Biol. *1210*, 203–227.

Sehgal, V.N., and Srivastava, G. (2007). Vitiligo: compendium of clinico-epidemiological features. Indian J. Dermatol. Venereol. Leprol. *73*, 149–156.

Shakhova, O., and Sommer, L. (2015). In vitro derivation of melanocytes from embryonic neural crest stem cells. In Methods in Molecular Biology (Humana Press), pp. 1–8.

Shin, J.M., Kim, M.Y., Sohn, K.C., Jung, S.Y., Lee, H.E., Lim, J.W., Kim, S., Lee, Y.H., Im, M., Seo, Y.J., et al. (2014). Nrf2 negatively regulates melanogenesis by modulating PI3K/Akt signaling. PLoS ONE *9*, e96035.

Slominski, A., Wortsman, J., Plonka, P.M., Schallreuter, K.U., Paus, R., and Tobin, D.J. (2005). Hair follicle pigmentation. J. Invest. Dermatol. *124*, 13–21.

Spiegelman, V.S., and Elcheva, I.A. (2017). Metabo-miR: miR-211 regulates mitochondrial energy metabolism in vitiligo. J. Invest. Dermatol. *137*, 1828–1830.

Takahashi, K., Tanabe, K., Ohnuki, M., Narita, M., Ichisaka, T., Tomoda, K., and Yamanaka, S. (2007). Induction of pluripotent stem cells from adult human fibroblasts by defined factors. Cell *131*, 861–872.

Tanimura, S., Tadokoro, Y., Inomata, K., Binh, N.T., Nishie, W., Yamazaki, S., Nakauchi, H., Tanaka, Y., McMillan, J.R., Sawamura, D., et al. (2011). Hair follicle stem cells provide a functional niche for melanocyte stem cells. Cell Stem Cell *8*, 177–187.

Tobin, D.J. (2011). The cell biology of human hair follicle pigmentation. Pigment Cell Melanoma Res. *24*, 75–88.

Wang, S., Zhou, M., Lin, F., Liu, D., Hong, W., Lu, L., Zhu, Y., and Xu, A. (2014). Interferon-γ induces senescence in normal human melanocytes. PLoS ONE *9*, e93232.

Whitton, M.E., Pinart, M., Batchelor, J., Leonardi-Bee, J., González, U., Jiyad, Z., Eleftheriadou, V., and Ezzedine, K. (2015). Interventions for vitiligo. Cochrane Database Syst. Rev. (*2*), CD003263.

Wind, B.S., Meesters, A.A., Kroon, M.W., Beek, J.F., van der Veen, J.P., Nieuweboer-Krobotová, L., Bos, J.D., and Wolkerstorfer, A. (2011). Punchgraft testing in vitiligo; effects of UVA, NB-UVB and 632.8 nm Helium-Neon laser on the outcome. J. Eur. Acad. Dermatol. Venereol. *25*, 1236–1237.

Yang, L., Wei, Y., Sun, Y., Shi, W., Yang, J., Zhu, L., and Li, M. (2015). Interferon-gamma inhibits melanogenesis and induces apoptosis in melanocytes: A pivotal role of CD8+ cytotoxic T lymphocytes in vitiligo. Acta Derm. Venereol. *95*, 664–670.

Yang, R., Zheng, Y., Li, L., Liu, S., Burrows, M., Wei, Z., Nace, A., Herlyn, M., Cui, R., Guo, W., et al. (2014). Direct conversion of mouse and human fibroblasts to functional melanocytes by defined factors. Nat. Commun. *5*, 5807.

STAR★METHODS

KEY RESOURCES TABLE

REAGENT or RESOURCE	SOURCE	IDENTIFIER
Antibodies		
Rabbit Polyclonal anti-NANOG	Genetex	Cat#GTX100863; RRID:AB_10615506
Goat Polyclonal anti-OCT4	Santa Cruz	Cat#SC-8628; RRID:AB_653551
Mouse Monoclonal anti-TRA-1-60	Millipore	Cat#MAB4360; RRID:AB_2119183
Mouse Monoclonal anti-SSEA4	DSHB	Cat#MC-813-70; RRID:AB_528477
Mouse Monoclonal anti-Nuclei (clone 235-1, hNuc)	Millpore	Cat#MAB1281
Mouse Monoclonal anti-TYR (clone T311)	Millpore	Cat#05-647; RRID:AB_94090
Mouse Monoclonal anti-TYRP1 (clone TA99)	Millpore	Cat#MABC592
Rabbit Monoclonal anti-TYRP1(clone 2340R, hTYRP1)	NSJ bioreagents	Cat#V3585SAF
Mouse Monoclonal anti-MITF	Sigma-Aldrich	Cat#M6065; RRID:AB_260607
Mouse Monoclonal anti-SOX10	Abcam	Cat#ab212843
Rabbit Polyclonal anti-PAX3 (hPAX3)	Atlas Antibodie	Cat#HPA063659; RRID:AB_2685080
Mouse Monoclonal anti-KRT15 (clone LHK15)	Millpore	Cat#CBL272; RRID:AB_11211790
Rat Monoclonal anti-ITGA6	Biolegend	Cat#313602; RRID:AB_345296
Cy3 Goat Anti-Rabbit IgG (H+L)	Jackson ImmunoResearch Labs	Cat#111-165-144; RRID:AB_2338006
Cy3 Goat Anti-Mouse IgG2b	Jackson ImmunoResearch Labs	Cat#115-165-207; RRID:AB_2338696
Cy3 Donkey Anti-Goat IgG (H+L)	Jackson ImmunoResearch Labs	Cat#705-165-003; RRID:AB_2340411
Cy3 Donkey Anti-Rabbit IgG	Jackson ImmunoResearch Labs	Cat#711-165-152; RRID:AB_2307443
Alexa Fluor® 647 Goat-Anti-Rat IgG (H+L)	Jackson ImmunoResearch Labs	Cat#112-605-167; RRID:AB_2338404
Alexa Fluor® 647 Donkey Anti-Mouse IgG (H+L)	Jackson ImmunoResearch Labs	Cat#715-605-150; RRID:AB_2340862
Alexa Fluor 555 Goat anti-Mouse IgG2a	Thermo Fisher Scientific	Cat#A21137; RRID:AB_2535776
Alexa Fluor 488 Goat anti-Mouse IgG1	Thermo Fisher Scientific	Cat#A21121; RRID:AB_2535764
Alexa Fluor 488 Goat anti-Mouse IgG2a	Thermo Fisher Scientific	Cat#A21131; RRID:AB_2535771
Biological Samples		
Human Epidermal Melanocytes (HEM-1, neonatal)	ScienCell	Cat#2210
Human Epidermal Melanocytes (HEM-2, adult)	Jiangsu University	N/A
Chemicals, Peptides, and Recombinant Proteins		
mTeSR	StemCell Technologies, Inc.	Cat#85850
AggreWell EB Formation Medium	StemCell Technologies, Inc.	Cat#05893
NutriStem XF/FF culture medium	Stemgent	Cat#01-0005
StemRNA-NM Reprogramming Kit	Stemgent	Cat#00-0076
Lipofectamine® RNAiMAX transfection reagent	Invitrogen	Cat#13778030
MCDB 201 Medium	Sigma-Aldrich	Cat#M6770
Non-Essential Amino Acids Solution	GIBCO	Cat#11140050
Basic fibroblast growth factor (bFGF)	Wako	Cat#068-04544
2-Mercaptoethanol	GIBCO	Cat#21985-023
Dexamethasone	Sigma-Aldrich	Cat#D4902
Insulin-transferrin-selenium	Sigma-Aldrich	Cat#I3146
Linoleic acid-bovine serum albumin	Sigma-Aldrich	Cat#L9530
12-O-tetradecanoyl-phorbel 13-acetate (TPA)	Sigma-Aldrich	Cat#P8139
L-ascorbic acid	Sigma-Aldrich	Cat#A4403
Stem cell factor (SCF)	R & D	Cat#255-SC-050
Endothelin-3	ENZO	Cat#ALX-155-003-PC05
Cholera toxin	Sigma-Aldrich	Cat#C8052

(*Continued on next page*)

Continued

REAGENT or RESOURCE	SOURCE	IDENTIFIER
Fetal bovine serum (FBS)	GIBCO	Cat#A3260802
Knockout serum replacement (KSR)	GIBCO	Cat#10828028
Polybrene	Sigma Aldrich	Cat#H9268
Mitomycin C	Sigma Aldrich	Cat#M4287
Y27632	Wako	Cat#253-00513
iMatrix-511	Stemgent	Cat#NP892-011
Fibronectin	BD Biosciences	Cat#356008
ACCUTASE	Innovative Cell Technologie	Cat#AT104-500
TrypLE Express	GIBCO	Cat#12604013
Collagenase type I	GIBCO	Cat#17100-017
TRIzol	Invitrogen	Cat#15596018
L-DOPA	Bomei	Cat#DD1054
Anti Asialo GM1	Wako	Cat#014-09801
Critical Commercial Assays		
RevertAid First Strand cDNA Synthesis Kit	Thermo Fisher Scientific	Cat#K1622
SYBR Premix Ex Taq Kit	Takara	Cat#RR420A
Masson-Fontana Kit	Solarbio	Cat#G2032
Deposited Data		
Raw data of RNA Sequencing	This paper	NCBI Short Read Archive: PRJNA492994
Experimental Models: Cell Lines		
L Wnt-3a cells	ATCC	CRL-2647; RRID:CVCL_0635
Experimental Models: Organisms/Strains		
Mouse: BALB/c Nude	Model Animal Research Center of Nanjing University	BALB/c Nude mice
Mouse: NOD/SCID	Model Animal Research Center of Nanjing University	NOD/SCID mice
Mouse: BALB/c	Jiangsu University	BALB/c mice
Oligonucleotides		
Primers for Real-time PCR, see Table S2	This paper	N/A
Recombinant DNA		
pMXs-hOCT3/4	Takahashi et al., 2007	Addgene Plasmid #17217
pMXs-hSOX2	Takahashi et al., 2007	Addgene Plasmid #17218
pMXs-hKLF4	Takahashi et al., 2007	Addgene Plasmid #17219
pMXs-hc-MYC	Takahashi et al., 2007	Addgene Plasmid #17220
Software and Algorithms		
HISAT2 (2.1.0)	Kim et al., 2015	RRID:SCR_015530 https://ccb.jhu.edu/software/hisat/index.shtml
StringTie (v1.3.4d)	Pertea et al., 2015	https://ccb.jhu.edu/software/stringtie/
Cluster 3.0	Eisen et al., 1998	http://bonsai.hgc.jp/%7Emdehoon/software/cluster/software.htm#ctv
Ingenuity® Pathway Analysis (IPA®) (44691306)	QIAGEN Inc.,	https://www.qiagenbioinformatics.com/products/ingenuity-pathway-analysis/

CONTACT FOR REAGENT AND RESOURCE SHARING

Further information and requests for resources and reagents should be directed to and will be fulfilled by the Lead Contact, Yun-Wen Zheng (ywzheng@md.tsukuba.ac.jp).

EXPERIMENTAL MODEL AND SUBJECT DETAILS

Information of Patients with Vitiligo

Number	Sex	Age (y)	Site
N2	Female	22	Thigh
N5	Male	45	Waist
N10	Female	36	Forehead

Fibroblasts of Patients

Under the permission of the Ethical Review Board of Affiliated Hospital of Jiangsu University (October 2014), as well as after having obtained necessary informed consent from all study subjects, freshly isolated skin specimens were obtained at the hospital. All experimental protocols for skin samples were approved by the ethics committee of Affiliated Hospital of Jiangsu University.

Skin tissue was collected after nevus resection of patients with halo nevus. The depigmented part was manually cut into smaller pieces and then transferred into 10-cm dishes. Culture medium consisting of DMEM/high glucose, 10% fetal bovine serum, and 1% penicillin/streptomycin was then added. The dishes were placed in an incubator for 4-5 days so that the tissue could adhere to the surface. Thereafter, half of the medium was replaced every 2 days. When 5 to 10 colonies comprising 50–100 cells formed, the medium was changed completely every 2 days. The fibroblasts were harvested when there were enough cells and then passaged.

Patient iPSC Lines

Patient iPS cell lines (JSDV) were generated by retroviral transduction where the retroviral vectors were prepared through calcium phosphate transfection of PlatE cells with pMX-vectors that harbored sequences encoding human OCT3/4, SOX2, KLF4, and c-MYC(Takahashi et al., 2007). Briefly, the virus-containing supernatant from PlatE cells was used to transduce patients' fibroblasts (passage 3-5, 10^5 cells were seeded in each well of a 6-well plate) in the presence of 4 μg/mL of polybrene. The medium was replaced 12 h later and the fibroblasts were allowed to recover for 48 h. Thereafter, they were seeded at a density of 3-4 × 10^4/well in a 6-well plate on mouse embryonic fibroblasts treated with mitomycin C. The culture medium used to maintain iPSCs contained DMEM/F12 supplemented with 20% KSR, 1 × non-essential amino acids solution, 4 ng/mL bFGF, 0.1mM 2-Mercaptoethanol and 1 × GlutaMAX. Colonies with typical iPSCs morphology were picked when they were large enough.

Non-integrating reprogramming was conducted using StemRNA-NM Reprogramming Kit. Briefly, fibroblasts were seeded at a density of 2 × 10^4/well in 6-well plates coated with iMatrix-511 in fibroblast culture medium. After 24 hours, the medium was switched to NutriStem™ XF/FF culture medium and NM-RNA cocktail was transfected using Lipofectamine® RNAiMAX™ transfection reagent. Four transfections were conducted and iPSC colonies were usually found on day 6-7.

Animal Studies

Male nude (BALB/c Nude) mice (5-7 weeks), NOD/SCID mice (4-6 weeks), and neonatal BALB/c mice (1-2 days after birth) were used in the experiments. All animal experiments were approved by the Laboratory Animal Management Committee of Jiangsu University (UJS-LAER-201510601)

METHOD DETAILS

Teratoma Formation

Feeder-free iPSCs were harvested and suspended in DMEM/F12. One quarter of the cells from a confluent 100-mm dish was injected into the testis of one NOD/SCID mouse. Teratoma were collected typically in 2-3 months and paraffin-embedded tissue was sectioned and stained with hematoxylin and eosin.

Uniform Embryoid Body Formation

iPSCs were maintained in feeder-free culture condition with mTeSR. A single-cell suspension of iPSCs was prepared with ACCUTASE™; Approximately 5 × 10^5 cells were added to each well in an Elplasia™ plate (24-well), and Y27632 was added to a final concentration of 10 μM. AggreWell EB Formation Medium was used. After 24 h, the aggregates were collected and cultured further in ultra-low attachment plates for 5-10 days.

Conventional Differentiation System

iPSCs maintained under a feeder-free culture condition were treated with TrypLE Express to generate small aggregates. These aggregates were cultured in ultra-low attachment plates with AggreWell EB Formation and 10 μM Y27632 was added in the first 24 hours. After 5-10 days, enlarged EBs were collected and plated on a fibronectin-coated plate for differentiation.

Suspension Differentiation System

EBs were collected and transferred to melanocyte differentiation medium (Fang et al., 2006) which contained conditioned medium from L-Wnt3a cells (50%), low-glucose DMEM (30%), MCDB 201 medium (20%), 0.05 μM Dexamethasone, 1 × insulin-transferrin-selenium, 1 × linoleic acid-bovine serum albumin, 10^{-4} M L-ascorbic acid, 50 ng/mL SCF, 100 nM Endothelial-3, 20 pM cholera toxin, 50 nM 12-O-tetradecanoyl-phorbel 13-acetate (TPA), and 4 ng/mL bFGF in ultra-low attachment plates. Half of the medium was replaced every 2-3 days. After two weeks, differentiated EBs were collected and plated on a fibronectin-coated plate. Cells were cultured for another 7 days and dissociated using TrypLE Express Enzyme and passaged. Differentiation medium with 0.5% FBS was used, but without TPA. Since then, iMelanocytes were passaged every 3-4 days.

Hair Follicle Reconstitution Assay

The protocol for isolation of neonatal mouse skin cells refers to the previous one (Lichti et al., 2008). First, truncal skins from 1-2-day-old BALB/c mice, a mouse strain without pigmentation, were removed and transferred into 0.25% cold trypsin in 10 cm dishes. Dishes with floating skins were stored at 4°C overnight in a refrigerator. Next day, they were transferred gently into a clean dish and epidermises were made to contact the dish and spread. Dermises were lifted up straight above the epidermises and transferred to a tube containing cold fibroblasts medium (DMEM/high glucose, 10% FBS and 1% penicillin /streptomycin) for later preparation of fibroblasts. Edges of epidermises were folded with forceps toward their centers, and each packet of epidermis was transferred to the dish containing cold epidermis medium (DMEM/high glucose, 8% FBS, 1.2 mM $CaCl_2$, and 1% penicillin /streptomycin).

Collected epidermises were minced with scissors. The resulting suspension was triturated by pipetting up and down more than ten times, and then was transferred to a 50 mL conical tube. Cell suspension was centrifuged at 200 g for 5 minutes and the supernatant including any floating stratum corneum pieces was carefully aspirated. Pellet in epidermis medium was resuspended and filtered through a 100-μm cell strainer. The collected cells were centrifuged again at 200 g for 5 minutes and pellet resuspend was suspended in epidermis medium. The total epidermal cell preparation included intrafollicular keratinocytes and hair follicle buds (aggregates).

The dermises were minced and incubated in 0.35% collagenase type I with agitation at 37°C in a shaking incubator (100 rpm) for 40 minutes. Then the digest was diluted with fivefold fibroblast medium and filtered through a 100-μm cell strainer. Filtrate was centrifuged at 300 g for 5 minutes and resuspended with fibroblasts medium. Subsequently, centrifugation was conducted five to six times (3 minutes for each time, low speed (50 g)) to remove most of hair follicles. Finally, it was centrifuged at 300 g (5 minutes) and resuspended with fibroblast medium.

Hair follicle reconstitution assays established by hypodermal injection were performed as described previously (Yang et al., 2014). The fresh cell mixtures were injected in 5-7-week-old male nude (BALB/c Nude) mice with hiMels. For each injection, 1×10^6 BALB/c neonatal dermal cells, 1×10^4 epidermal aggregates and 0.5×10^6 hiMels were used. In addition, 0.5×10^6 human fibroblasts and normal HEM were mixed with mouse cells as controls instead of hiMels. At week 2, the reconstituted skin tissues were harvested and embedded in OCT compound.

In hair follicle reconstitution assays established by the chamber method (Lichti et al., 2008), a portion of back skin was removed with scissors to create a 1-cm diameter hole. Then the rim of chamber was inserted under the skin and was clipped to the chamber with autoclips, to prevent the chamber from popping out of the hole. Cell suspension was ejected through the hole of the dome onto the graft area using the Pipetman. 5×10^6 dermal cells, 5×10^4 epidermal aggregates and 2.5×10^6 hiMels were transplanted in one chamber for each mouse. Chambers were removed 7 days after grafting. At different time points, the reconstituted tissues were harvested and embedded in OCT compound.

Real-time PCR

Total RNA was isolated using TRIzol and reverse transcribed into cDNA using a RevertAid First Strand cDNA Synthesis Kit according to the manufacturer's instructions. Amplification was performed on a real-time PCR system (Applied Biosystems QuantStudio 3, USA). The whole procedure was according to the manual of SYBR Premix Ex Taq kit. Gene expression levels were normalized to that of GAPDH and were quantified based on the ΔCt method.

RNA Sequencing

Total RNA was extracted using TRIzol reagent following the manufacturer's procedure. The libraries of ViMel-1, ViMel-2, JSDV-5, HEM-1 were sequenced using 150-bp paired-end sequencing on an Illumina HiSeq 4000 instrument. The libraries of the rest samples were sequenced using 150-bp paired-end sequencing on an Illumina HiSeq X Ten instrument. All paired-end reads of each sample were trimmed and quality filtered via fastp 0.18.0. HISAT2 2.1.0 (Kim et al., 2015)was used to map the filtered reads against the human reference sequence (hg 38). Mapped reads were counted and then transcript abundance was measured in FPKM (fragments per kilobase of transcript per million fragments mapped) units using StringTie (v1.3.4d)(Pertea et al., 2015)

Bioinformatics for RNA Sequencing Data

Differentially expressed (fold change of FPKM value > 2 or < 0.5) gene profiles between iPSCs and melanocytes, and genes involved in the differentiation of melanocytes (Mort et al., 2015) were normalized (Z-score normalized FPKM values) for heatmap which was generated using pheatmap package in R. K-means cluster was performed in Cluster 3.0(Eisen et al., 1998). Common genes expressed in patient iMel and HEM were selected for Venn diagram. Scatterplots were generated by using ggplot2 in R. Differentially

expressed (fold change of FPKM value > 2 or < 0.5) gene profiles between patient iMels and HEM-1 were analyzed by Ingenuity® Pathway Analysis (IPA®) to identify the most significant pathways and discover potential regulatory networks associated with patient iMels.

Immunocytochemistry

Cells or frozen tissue samples were fixed with 4% paraformaldehyde for 15 minutes (4°C), and then washed and permeabilized three times with PBST (0.5% Tween20 in PBS) (5 minutes for each time, RT). Normal goat serum was used as a blocking reagent to reduce background for 1 hour (RT). After incubation with primary antibody overnight (4°C), samples were subsequently incubated with the second antibody for 1 hour (room temperature). Optical sections of the cells were observed under a Nikon-ECLIPSE Ti-S fluorescence microscope (Nikon, Japan). The dilution ratio for primary antibodies is as follows: OCT4 (Santa Cruz, 1:100), NANOG (Genetex, 1:200), TRA-1-60 (Millipore, 1:100), SSEA4 (DSHB, 1:100), TYR (Millipore, 1:100); TYRP1 (Millipore, 1:200); TYRP1 specific for human (NSJ bioreagents, 1:200); MITF (Sigma-Aldrich, 1:200); SOX10 (Abcam, 1:250); PAX3(Atlas Antibodie,1:100); Anti-Nuclei antibody specific for human (Millipore, 1:500); KRT15 (Millipore, 1:100); ITGA6 (Biolegend, 1:200). The dilution ratio for all the second antibodies is 1:500.

L-DOPA Staining

Cells or tissue sections were fixed with 4% paraformaldehyde and incubated in a 0.1% solution of L-DOPA in PBS for 3-4 hours at 37°C. The nuclei were stained with hematoxylin and sections were thoroughly dehydrated in absolute alcohol.

Masson-Fontana Staining

Masson-Fontana kit was used. Briefly, cells or tissue sections were fixed with 4% paraformaldehyde and then treated with ammoniacal silver nitrate solution in a closed jar for 40 minutes at 56°C. Samples were washed well in ddH_2O and treated with hypo solution for 5 minutes. Then, samples were counterstained with neutral red stain for 5 minutes and rinsed in ddH_2O. Finally, the preparations were thoroughly dehydrated.

QUANTIFICATION AND STATISTICAL ANALYSIS

Statistical and graphical data analyses were performed using Microsoft Excel and Prism 5 (Graphpad) software. Data are presented as means ± SD. Student's t tests was used to calculate P values where appropriate. $p < 0.05$ was considered to be significant.

DATA AND SOFTWARE AVAILABILITY

The accession number for the RNA-sequencing data reported in this paper is NCBI Short Read Archive: PRJNA492994.